Hydride Transfer and Dihydrogen Elimination from Osmium and Ruthenium Metalloporphyrin Hydrides: Model Processes for Hydrogenase Enzymes and the Hydrogen Electrode Reaction

James P. Collman,* Paul S. Wagenknecht, and Nathan S. Lewis†

Contribution from the Department of Chemistry, Stanford University, Stanford, California 94305.
Received October 23, 1991

Abstract: A series of metalloporphyrin hydride complexes of the type K[M(Por)(L)(H)] (M = Ru, Os; Por = OEP, TMP; L = THF, *Im, PPh_3, pyridine) has been synthesized by stoichiometric protonation of the corresponding K_2[M(Por)], followed by addition of L. The addition of excess acids to these hydrides resulted in the elimination of dihydrogen. The kinetics showed no evidence for a bimolecular mechanism for this process and suggest simple protonation of the metal–hydride bond followed by dihydrogen loss. One-electron oxidation of the metal hydrides also resulted in dihydrogen formation. The kinetics of the oxidatively induced hydrogen evolution step from K[Ru(OEP)(THF)(H)] were examined and indicate a bimolecular mechanism in which two metal hydrides reductively eliminate one dihydrogen molecule. The rate constant was determined to be 88 ± 14 M^{-1} s^{-1}. These reaction mechanisms are discussed in the context of designing bimetallic proton reduction catalysts. The metal hydride K[Ru(OEP)(THF)(H)], was also synthesized by heterolytic activation of H_2. This hydride is a good one-electron reductant (−1.15 V vs $FeCp_2$) and is capable of reducing, by hydride transfer, the NAD^+ analogue, 1-benzyl-*N*,*N*-diethylnicotinamide. This nicotinamide reduction by a hydride formed from heterolytic dihydrogen activation is suggested as the mechanism for hydrogenase enzymes.

Transition metal hydrides are of great interest because of their intimate connection with the recently discovered η^2-dihydrogen complexes. Heterolytic activation of the dihydrogen ligand, resulting in metal hydrides, has been reported by several groups.[1-3] Reactive metal hydrides formed from heterolytic dihydrogen activation have been proposed as the intermediates in the dihydrogen uptake catalyzed by hydrogenase enzymes.[4] Hydrogenase enzymes utilize the reducing capabilities of dihydrogen to reduce cofactors, such as NAD^+, that are involved in the metabolic electron transfer chains. Successful transition metal based mimics of these enzymes will require formation of metal hydrides capable of reducing such cofactors.

Transition metal hydrides have also attracted interest because of their intermediacy in the catalysis of proton reduction at metal surfaces.[5] Recently, soluble cobalt macrocycles have also been observed to catalyze dihydrogen evolution from aqueous solutions that contain a sacrificial electron donor.[6,7] Cobalt hydrides have been suggested as the intermediates in these processes. Regardless of the metal involved, the general reaction sequence of the dihydrogen production is suggested to proceed through two parallel routes: (1) bimolecular reductive elimination of dihydrogen from two metal hydrides, and (2) protonation of a metal hydride fragment, followed by dihydrogen elimination. The design of homogeneous catalysts for proton reduction will require a detailed knowledge of these mechanisms, as well as an understanding of the factors governing the stability of these metal hydrides and the rate of hydrogen evolution from such intermediates.

Herein, we report the synthesis of several stable anionic metalloporphyrin hydrides. Our interest in these hydrides is 2-fold. We will probe their reducing capabilities in an attempt to mimic hydrogenase catalyzed substrate reduction. And, we will analyze the mechanisms and rates of hydrogen elimination pathways for several of these hydrides with varying electronic and steric environments.[8]

Results

Synthesis of the Metalloporphyrin Hydrides. Synthesis of the metalloporphyrin hydride anions of the type K[M(Por)(L)(H)] (M = Ru, Os; Por = OEP, TMP; L = THF, *Im, PPh_3, py)[9] was achieved by protonation of the metalloporphyrin dianions, K_2[M(Por)], according to modified literature procedures.[10,11] These procedures yield metalloporphyrin hydrides with a labile THF in the trans position. In THF-d_8 solvent, the THF ligand was not observed due to solvent exchange. The presence of axially bound THF was inferred by the observation that the addition of stronger ligands, i.e., *Im, pyridine, and PPh_3, resulted in their binding trans to the hydride (as indicated by ^{1}H NMR), indicating a tendency for these hydrides to acquire an octahedral geometry. (We observe an empirical ordering of ligand binding affinities: PPh_3, *Im, py > THF > H_2O.) The anionic metal hydride K[Ru(OEP)(THF)(H)] has also been prepared by stirring Ru(OEP)$(THF)_2$ in THF solution with a large excess of KOH under 1 atm of dihydrogen (eq 1). The product metal hydride likely results from deprotonation of a transient dihydrogen complex, Ru(OEP)(THF)(H_2).[3]

Reactivity of K[Ru(OEP)(L)(H)]. The anionic K[Ru(OEP)(THF)(H)] is very stable both in THF solution and as a

† Division of Chemistry and Chemical Engineering, California Institute of Technology, Pasadena, CA 91125.

(1) (a) Chinn, M. S.; Heinekey, D. M.; Payne, N. G.; Sofield, C. D. *Organometallics* **1989**, *8*, 1824–1826. (b) Jia, G.; Morris, R. H. *Inorg. Chem.* **1990**, *29*, 581–582. (c) Jia, G.; Morris, R. H.; Schweitzer, C. T. *Inorg. Chem.* **1991**, *30*, 593–594. (d) Jia, G.; Morris, R. H. *J. Am. Chem. Soc.* **1991**, *113*, 875–883. (e) Crabtree, R. H.; Lavin, M.; Bonneviot, L. *J. Am. Chem. Soc.* **1986**, *108*, 4032–4037. (f) Chinn, M. S.; Heinekey, D. M. *J. Am. Chem. Soc.* **1987**, *109*, 5865–5867. (g) Chinn, M. S.; Heinekey, D. M. *J. Am. Chem. Soc.* **1990**, *112*, 5166–5175.

(2) Kristjánsdóttir, S. S.; Norton, J. R. Acidity of Hydrido Transition Metal Complexes in Solution. In *Transition Metal Hydrides: Recent Advances in Theory and Experiment*; Dedieu, A., Ed.; VCH: New York, 1991; pp 309–359.

(3) Preceding paper in this issue.

(4) (a) Krasna, A. I.; Rittenberg, D. *J. Am. Chem. Soc.* **1954**, *76*, 3015–3020. (b) Crabtree, R. H. *Inorg. Chim. Acta* **1986**, *125*, L7–L8.

(5) Wendt, H.; Plzak, V. In *Electrochemical Hydrogen Technologies: Electrochemical Production and Combustion of Hydrogen*; Wendt, H., Ed.; Elsevier: Amsterdam, 1990; pp 15–62.

(6) Kellett, R. M.; Spiro, T. G. *Inorg. Chem.* **1985**, *24*, 2373–2377.

(7) Connolly, P.; Espenson, J. H. *Inorg. Chem.* **1986**, *25*, 2684–2688.

(8) We have published pieces of this work on metalloporphyrin hydrides in two communications: (a) Collman, J. P.; Wagenknecht, P. S.; Hembre, R. T.; Lewis, N. S. *J. Am. Chem. Soc.* **1990**, *112*, 1294–1295. (b) Collman, J. P.; Hutchison, J. E.; Wagenknecht, P. S.; Lopez, M. A.; Guilard, R.; Lewis, N. S. *J. Am. Chem. Soc.* **1990**, *112*, 8206–8207.

(9) Abbreviations: OEP = octaethylporphyrinato dianion; TMP = *meso*-tetramesitylporphyrinato dianion; THF = tetrahydrofuran; *Im = 1-*tert*-butyl-5-phenylimidazole; PPh_3 = triphenylphosphine; NAD^+ = nicotinamide adenine dinucleotide (oxidized form); $FeCp_2$ = ferrocene.

(10) Venburg, G. D. Ph.D. Thesis 1990, Stanford University.

(11) Collman, J. P.; Brothers, P. J.; McElwee-White, L.; Rose, E. *J. Am. Chem. Soc.* **1985**, *107*, 6110–6111.

0002-7863/92/1514-5665$03.00/0

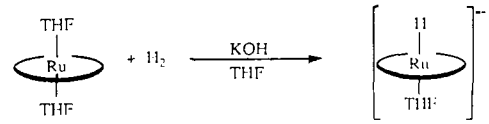

(1)

solid; it cannot be induced to reductively eliminate dihydrogen. Heating the hydride at reflux in 3:1 toluene:THF resulted in very little degradation. Even vacuum pyrolysis of a lyophylized powder of K[Ru(OEP)(THF)(H)] at 205 °C for 10 h did not appreciably degrade the complex (eq 2). The products expected from an elimination reaction are H_2 and K[Ru(OEP)].

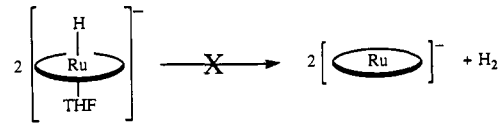

(2)

It is instructive to think about the microscopic reverse of this elimination which would comprise the addition of dihydrogen to a ruthenium porphyrin anion, K[Ru(OEP)]. This ruthenium(I) monomer has never been observed; only the product of its dimerization, $K_2[Ru(OEP)]_2$, has been prepared, in moderate yield, by incomplete potassium metal reduction of $[Ru(OEP)]_2$ in THF.[10] When treated with 1 atm of H_2 in THF, $K_2[Ru(OEP)]_2$ oxidatively added dihydrogen across the metal–metal bond to yield K[Ru(OEP)(THF)(H)] (eq 3). Such reactivity is not uncommon for homonuclear metal–metal bonds.[12]

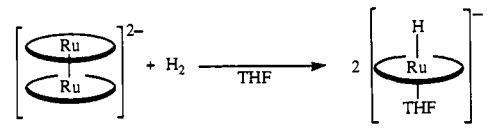

(3)

Protonation of millimolar solutions of K[Ru(OEP)(THF)(H)] with 1 equiv of PhCOOH in THF resulted in immediate and quantitative formation of dihydrogen. Protonation using 200 equiv of H_2O required over 1 h to proceed to completion (eq 4). To

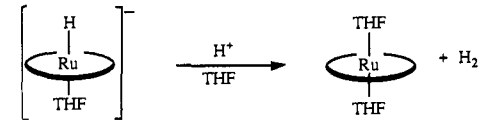

(4)

determine if there is a bimolecular component to this H_2 elimination reaction, the K[Ru(OEP)(THF)(H)] was protonated with 200 equiv of D_2O, and the evolved hydrogen gases were analyzed for H_2, HD, and D_2 by gas chromatography. (Dihydrogen formation by prior protonation of the site trans to the hydride would likely require a bimolecular step.) The H_2:HD:D_2 ratio was approximately 0:2:1. Because bimolecular pathways are expected to yield some H_2, these data indicate that bimolecular pathways (under the conditions of these experiments) are slow or non-existent. The presence but not predominance of D_2 gas indicates that some exchange between the hydride and D_2O occurred, but that the exchange was slower than the dihydrogen elimination rates.

When the axial THF was replaced with pyridine to form K[Ru(OEP)(py)(H)], the protonation reaction with H_2O in THF occurred immediately and yielded an asymmetric product formulated as Ru(OEP)(py)(THF) based on ^1H NMR data. Additionally, when D_2O was used as the acid, only HD gas was formed. Neither H_2 nor D_2 was observed, indicating that no exchange had occurred. The lack of H_2 and D_2 also indicates that bimolecular elimination processes were not rapid in this system.

Reduction of Substrates by K[M(Por)(L)(H)]. The anionic hydrides were also investigated for reducing properties as either hydride transfer or 1 e^- transfer reagents. Because of relevance to the electron transfer chains in hydrogenase catalyzed dihydrogen activation,[13] an NAD^+ analogue was studied as a hydride acceptor

(12) Collman, J. P.; Hegedus, L. S.; Norton, J. R.; Finke, R. G. *Principles and Applications of Organotransition Metal Chemistry*, 2nd ed.; University Science Books: Mill Valley, CA, 1987; p 86.

Table I. Potentials for the Oxidations of Metal Hydrides, K[M(Por)(L)(H)], in THF with 0.2 M $TBAPF_6$ as Backing Electrolyte[a]

K[M(Por)(L)(H)]	$E_{1/2}(M^{III/II})$ vs. $Fe(Cp_2)^{+/0}$
K[Ru(OEP)(THF)(H)	−1.15 V
K[Ru(OEP)(*Im)(H)]	−1.21 V
K[Ru(TMP)(THF)(H)]	−1.18 V
K[Os(OEP)(THF)(H)]	−1.50 V

[a] Potentials are referenced vs. an internal ferrocene standard.

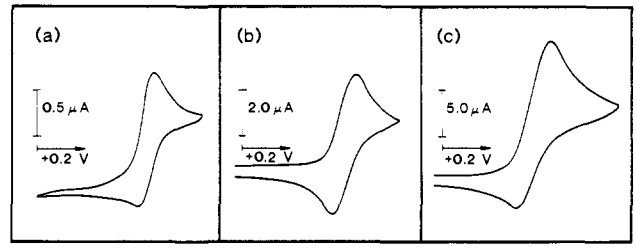

Figure 1. Dependence of the shape of the cyclic voltammograms of K[Ru(OEP)(THF)(H)] for varying scan rates and concentrations: (a) 2.0 mM, 10 mV/s; (b) 2.0 mM, 100 mV/s; (c) 7.6 mM, 100 mV/s.

for the K[Ru(OEP)(THF)(H)] complex. When a stoichiometric amount of the NAD^+ analogue, [1-benzyl-*N*,*N*-diethylnicotinamide]PF_6, was introduced to a solution of K[Ru(OEP)(THF)(H)] in THF-d_8, a species with broad ^1H NMR resonances was observed. Addition of a drop of pyridine to this mixture yielded both $Ru(OEP)(py)_2$ and the reduced nicotinamide, 1-benzyl-*N*,*N*-diethyl-1,6-dihydronicotinamide (eq 5), as detected by ^1H NMR. When the ruthenium deuteride, K[Ru(OEP)-

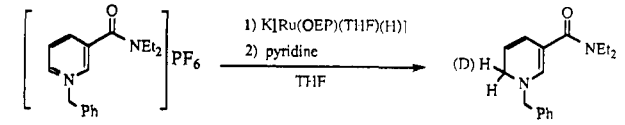

(5)

(THF)(D)], was used instead of the hydride, the corresponding deuterated dihydronicotinamide was produced with the deuterium incorporated in the 6-position of the pyridinium ring, as demonstrated by the splitting pattern in the ^1H NMR. When 1-benzyl-*N*,*N*-diethyl-1,4-dihydronicotinamide was treated with $Ru(OEP)(THF)_2$, no isomerism to the 1,6-dihydronicotinamide was noted. This suggests that the 1,6-dihydronicotinamide formed in the hydride transfer reaction is the kinetic product and is not a result of initial 1,4-transfer, followed by a metalloporphyrin catalyzed [1,3]-sigmatropic shift.

The hydrides, K[Ru(OEP)(THF)(H)], K[Ru(OEP)(*Im)(H)], K[Ru(TMP)(THF)(H)], and K[Os(OEP)(THF)(H)], each reduced $[Fe(Cp)_2]PF_6$ to ferrocene. The reduction potentials of the M(III/II) couples (vs. ferrocene) in THF are listed in Table I.

Cyclic Voltammetry of K[M(Por)(L)(H)]. Cyclic voltammograms of the first oxidation wave of THF solutions of 2.0 mM K[Ru(OEP)(THF)(H)] were recorded at several scan rates (20 to 200 mV/s). Parts a and b of Figure 1 show the cases at 10 and 100 mV/s. At fast scan rates the electrode process appeared reversible, but as the scan rate was reduced, the absolute value of the ratio of the cathodic peak current to the anodic peak current, i_{pc}/i_{pa}, decreased (Figure 1, a and b). This behavior is indicative of an E_rC_i process, i.e., one in which the reversible charge transfer process, E_r, is followed by an irreversible chemical step, C_i, which partially depletes the electroactive species before the completion of the return scan.[14]

Cyclic voltammograms at a single scan rate, 100 mV/s, for a series of K[Ru(OEP)(THF)(H)] concentrations (2, 4, and 7.6

(13) Schlegel, H. G.; Schneider, K. In *Hydrogenases: Their Catalytic Activity, Structure and Function*; Schlegel, H. G., Schneider, K., Eds.; Verlag–Erich Goltze KG: Göttingen, 1978; pp 15–44.

(14) Bard, A. J.; Faulkner, L. R. In *Electrochemical Methods: Fundamentals and Applications*; John Wiley and Sons, Inc.: New York, 1980; pp 429–487.

mM) also displayed variable peak current ratios. Scans obtained using the lowest and highest K[Ru(OEP)(THF)(H)] concentrations are displayed in Figure 1, parts b and c, respectively. The decrease in i_{pc}/i_{pa} as a function of increasing concentration of the metal hydride is indicative of an E_rC_i process in which the chemical reaction order is greater than one with respect to the metal hydride.[15] If the chemical decomposition step were first order in metal, the observed peak current ratios would have been invariant as a function of concentration of the hydride.[16]

The products of the irreversible chemical step, C_i, were determined by exhaustive one-electron oxidation of K[Ru(OEP)(THF)(H)] in a cell sealed with a rubber septum. The exhaustive electrolysis yielded $Ru(OEP)(THF)_2$ and dihydrogen gas, as determined by UV–vis spectroscopy and gas chromatography, respectively.

Cyclic voltammetry of the 1-*tert*-butyl-5-phenylimidazole adduct, K[Ru(OEP)(*Im)(H)], indicated similar reactivity to that found for K[Ru(OEP)(THF)(H)]. The peak current ratio, i_{pc}/i_{pa}, decreased with decreasing scan rates and also decreased with increasing metal hydride concentration. This is again indicative of an E_rC_i process involving a chemical step with a reaction order greater than one with respect to the hydride. However, under comparable conditions, the rates of the chemical step following oxidation of the imidazole complex were larger than those for the THF complex. These accelerated rates relative to the rates for K[Ru(OEP)(THF)(H)] indicate that replacement of THF with *Im accelerates the chemical decomposition.

When OEP was replaced with the bulkier TMP to form K[Ru(TMP)(THF)(H)], voltammetric peak current ratios indicating an E_rC_i processes were perceptible only at the slowest scan rates, indicating that chemical decomposition of this complex was much slower than that for K[Ru(OEP)(THF)(H)]. Similarly, voltammetry of K[Os(OEP)(THF)(H)] did not yield changes in the i_{pc}/i_{pa} ratio over the range of scan rates investigated in this work.

Chemical Oxidations of K[M(Por)(L)(H)]. The stoichiometry of dihydrogen production from oxidation of the metal hydride anions was determined in THF using insoluble VBr_3 as the oxidant. This oxidant was chosen because more powerful oxidants such as ferricinium ion caused some degradation of the metalloporphyrin.[17] Stoichiometry measurements were performed by injecting THF-d_8 solutions of the hydrides into sealed vials that contained a stir bar and 2 to 3 equiv of VBr_3. For most of the metal hydrides a color change was observed within 1 min, indicating that some reaction had occurred. After the solution was stirred for approximately 45 min, the headspace was analyzed for H_2 by gas chromatography, and the solution was analyzed by ^1H NMR spectroscopy. The porphyrin concentration was determined relative to an internal standard. For the hydrides K[Ru(OEP)(THF)(H)], K[Ru(OEP)(*Im)(H)], and K[Ru(OEP)(PPh_3)(H)], stoichiometric amounts (±15%) of H_2 and of Ru(OEP)(L)(THF) [L = THF, *Im, PPh_3] were observed as a result of this reaction (eq 6).

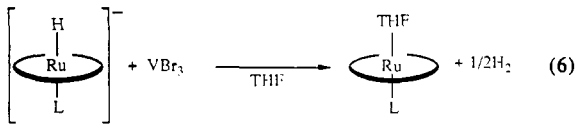

(6)

Product stoichiometries for oxidation of hydride complexes that decomposed more slowly, or not at all, displayed substantial decomposition of the porphyrin and incomplete dihydrogen formation. In particular, oxidation of K[Ru(TMP)(THF)(H)] in THF using VBr_3 yielded ca. 50% of the expected H_2 and less than 50% of the expected $Ru(TMP)(THF)_2$. Oxidation of the K[Os(OEP)(THF)(H)] with VBr_3 yielded nearly stoichiometric quantities of H_2 after 16 h of stirring but uncharacterized porphyrinic products. Treatment of K[Os(OEP)(THF)(H)] with 1 equiv of $[Fe(Cp)_2]PF_6$ resulted in immediate and clean oxidation to a paramagnetic species; the resulting paramagnetic complex closely resembles the known paramagnetic Os(OEP)(Me),[10] which is an isoelectronic analogy to the neutral Os(OEP)(THF)(H) that is expected from oxidation of the anionic osmium hydride. This paramagnetic species decomposed very slowly ($t_{1/2} \sim 1$ day) in THF, yielding less than 50% of the expected dihydrogen and producing $[Os(OEP)]_2$ as the only observed porphyrinic product.

Although the reaction of K[Ru(OEP)(THF)(H)] with $[Fe(Cp)_2]PF_6$ led to some decomposition of the metal hydride, we performed this oxidation at low temperature (−78 °C) and followed the decomposition by ^1H NMR spectroscopy while warming the sample. Ferricinium was used as the oxidant for the NMR study because its partial solubility in organic solvents allowed more accurate stoichiometric additions and more rapid electron transfer than VBr_3. The major products of oxidation, before warming the sample, were ferrocene and a paramagnetic ruthenium porphyrin. The ^1H NMR of the paramagnetic complex closely resembled Ru(OEP)(Me),[10] which is a characterized isoelectronic analogue of Ru(OEP)(H). On the basis of this evidence, it is likely that ferricinium oxidizes the anionic ruthenium hydride and that the observed paramagnetic species is the neutral ruthenium(III) hydride, Ru(OEP)(H). Upon warming, this species decomposed, forming the characterized η^2-dihydrogen complex Ru(OEP)(THF)(H_2)[3] as a major product.

Kinetics of Hydride Decomposition Following Oxidation. Analyses by UV–vis spectroscopy of the kinetics of the chemical step following K[M(Por)(L)(H)] oxidation were hampered by the inability to find a suitable *soluble* oxidant. Similarities between the reactant and product spectra also hampered optical measurements. Furthermore, some of the reactions are too fast to determine rate constants accurately by ^1H NMR spectroscopy. The observed dependence of the cyclic voltammograms on the metal hydride concentration and scan rate suggested that electrochemical techniques would provide quantitative information for this reaction. Furthermore, electrochemical methods overcome the aforementioned problems: A soluble oxidant is not needed because the electrode serves as the oxidant, and electrochemical techniques allow reactions with half-lives between milliseconds and tens of seconds to be measured conveniently.[14]

The electrochemical techniques require that the products of decomposition are not electroactive at potentials where the reactant species is electroactive. For example, quantifying the rate of the chemical step in the following EC mechanism

$$R^- - e^- \rightarrow O \rightarrow P \qquad (7)$$

requires that P is not electroactive at the potential at which R^- is oxidized. The K[Ru(Por)(L)(H)] systems are ideally suited for such a study because they are oxidized at potentials well negative of NHE, whereas the corresponding ruthenium(II) metalloporphyrins with neutral base ligands are oxidized at potentials near or positive of NHE.[18] Due to the simplicity of the measurements and the accuracy of the technique, we chose to use double potential step chronoamperometry (DPSCA) to obtain rate information rather than potential sweep techniques such as cyclic voltammetry.

Theoretical Working Curves for DPSCA of a Dimerization Process. The general method of DPSCA for determining the kinetics of a chemical reaction following an oxidation involves the following:[19] (1) The working electrode is stepped to some potential at which oxidation of the electroactive species ($R^- - e^- \rightarrow O$) is diffusion controlled. (2) The electrode is held at that potential for some time, τ, and then (3) stepped back to a potential at which

(15) Olmstead, M. L.; Hamilton, R. G.; Nicholson, R. S. *Anal. Chem.* **1969**, *41*, 260–267.
(16) Nicholson, R. S.; Shain, I. *Anal. Chem.* **1964**, *36*, 706–723.
(17) Ferricenium is an excellent radical trap and may react with the hydride radical formed. Collman, J. P.; Hegedus, L. S.; Norton, J. R.; Finke, R. G. *Principles and Applications of Organotransition Metal Chemistry*, 2nd ed.; University Science Books: Mill Valley, CA, 1987; p 173.
(18) Kadish, K. M. In *Progress in Inorganic Chemistry*; Lippard, S. H., Ed.; John Wiley and Sons, Inc.: New York, 1986; Vol. 34, pp 435–605.
(19) Bard, A. J.; Faulkner, L. R. In *Electrochemical Methods: Fundamentals and Applications*; John Wiley and Sons, Inc.: New York, 1980; pp 176–183.

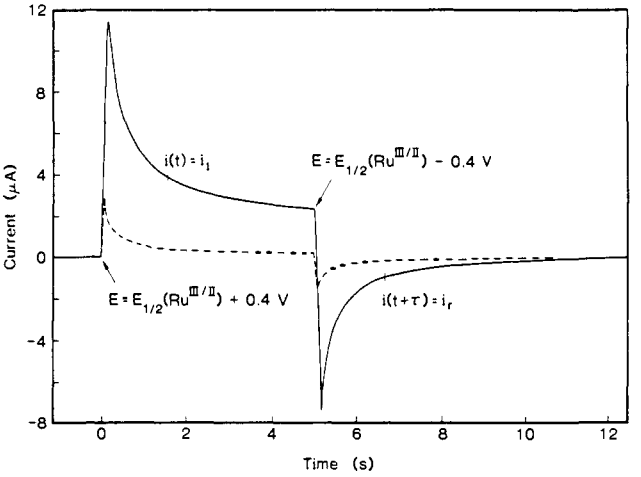

Figure 2. Double potential step chronoamperometric scan for a 3.5 mM solution of K[Ru(OEP)(THF)(H)]. At $t = 0$, a potential 400 mV positive of $E_{1/2}(Ru^{III/II})$ is applied. This potential is maintained for τ = 5 s and then a potential 400 mV negative of $E_{1/2}$ is applied. (—) Scan of hydride; (---) blank.

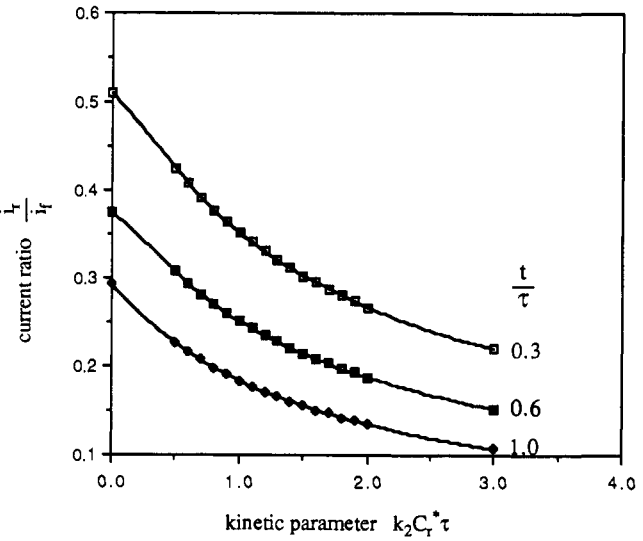

Figure 3. DPSCA theoretical working curves for a chemical dimerization following the electron transfer. C_r^* is the bulk concentration of the electroactive species, and k_2 is the second-order rate constant of dimerization.

the reduction of the oxidized species ($O + e^- \rightarrow R^-$) is diffusion controlled. Longer holding times, τ, allow more time for chemical decomposition of the oxidized species ($O \rightarrow P$) and will therefore produce higher forward to reverse current ratios. One common method for analyzing DPSCA data is to tabulate the current (i_f) at some time, t (where $t < \tau$), in the forward potential step and to also tabulate the current (i_r) at time $t + \tau$ in the reverse step (see Figure 2). The current ratio, i_r/i_f, is then used to obtain kinetic information. (i_r/i_f is a negative quantity. We will use i_r/i_f to refer to the absolute value of the current ratio.)

This current relationship, i_r/i_f, has been related to a first-order kinetic parameter for varying t/τ values.[20] Several groups[21] have used DPSCA to determine second-order parameters, but we were unable to locate working curves in the literature for the second-order dimerization processes in a format that could be compared to the first-order working curves of Schwarz and Shain.[20] We therefore used previously published calculations[22] to derive these working curves for a second-order dimerization (see Figure 3 and Appendix) and analyzed our data for the DPSCA experiments with respect to both a first-order decay and a second-order decay. This analysis should reveal whether the hydrogen elimination is unimolecular or bimolecular with respect to the metal.

Table II. Comparison of First- and Second-Order Rate Constants Derived from DPSCA of K[Ru(OEP)(THF)(H)] at 1.9, 3.8, and 7.6 mM Ru(H) Concentrations

	1.9 mM		3.8 mM		7.6 mM	
τ, s	k_1 (s^{-1})	k_2 (M^{-1} s^{-1})	k_1 (s^{-1})	k_2 (M^{-1} s^{-1})	k_1 (s^{-1})	k_2 (M^{-1} s^{-1})
2	0.050	71	0.14	87	0.29	95
4					0.23	92
5	0.070	83	0.14	97		
6					0.20	90
8					0.17	*a*
10	0.063	89	0.11	93	0.15	*a*
12					0.13	*a*
15					0.11	*a*
20	0.050	84	0.07	*a*		

[a] Current ratios were too small to extrapolate plots to obtain a kinetic parameter.

Table III. Comparison of First- and Second-Order Rate Constants Derived from DPSCA of K[Ru(OEP)(*Im)(H)] at 2.0 and 3.9 mM Ru(H) Concentrations

	2.0 mM		3.9 mM	
τ, s	k_1 (s^{-1})	k_2 (M^{-1} s^{-1})	k_1 (s^{-1})	k_2 (M^{-1} s^{-1})
2	0.32	430	0.40	300
3			0.35	310
4	0.21	320	0.30	300
5			0.24	270
6	0.16	250	0.23	*a*
8	0.13	230	0.19	*a*
10	0.12	240		

[a] Current ratios were too small to extrapolate plots to obtain a kinetic parameter.

DPSCA of the Metalloporphyrin Hydrides. Three solutions of K[Ru(OEP)(THF)(H)] were analyzed: 1.9 mM, 3.8 mM, and 7.6 mM. DPSCA was performed on each solution using τ values ranging from 2 to 20 s (see, for example, Figure 2, τ = 5 s). Current ratios were taken for t/τ values of 0.3 (this was a convenient time because it was far enough into the trace to allow the pen of the X–Y recorder to "catch up" but was near enough to the potential step to produce a substantial current), and first- and second-order kinetic parameters were then obtained from the working curves (Figure 3). The rate constants obtained from these analyses are presented in Table II. Treating the chemical step following the oxidation as first order with respect to the metal hydride resulted in a rate constant that approximately doubled upon doubling the concentration. Using this approach there was also a decrease in the calculated first-order rate constant as τ increased. These discrepancies suggest that the reaction order is higher than unity. Treating the chemical reaction as second order yielded rate constants with much less variance. These data clearly establish that the chemical decomposition is second order with respect to the metal hydride.

These same experiments were performed on the K[Ru(OEP)(*Im)(H)]. The data are presented in Table III. These data also demonstrate a decrease in the calculated first-order rate constant with increasing τ and an increase in k_1 with increasing concentration. With the exception of the k_2 value of 430 M^{-1} s^{-1} at τ = 2 s (for short delay times the resulting speed of the plotter pen is responsible for some error), the second-order rate constants exhibited much less variance than the first-order rate constants.

(20) Schwarz, W. M.; Shain, I. *J. Phys. Chem.* **1965**, *69*, 30–40.

(21) Several authors have used DPSCA to obtain rate information concerning dimerization reactions, but, to our knowledge, none have published simple working curves analogous to those for the first-order kinetics by Schwarz and Shain[20] so that first- and second-order kinetics may easily be compared. (a) Jensen, M. A.; Elving, P. J. *Biochim. Biophys. Acta* **1984**, *764*, 310–315. (b) Childs, W. V.; Maloy, J. T.; Keszthelyi, C. P.; Bard, A. J. *J. Electrochem. Soc.* **1971**, *118*, 874–880. (c) Amatore, C.; Garreau, D.; Hammi, M.; Pinson, J.; Savéant, J.-M. *J. Electroanal. Chem.* **1985**, *184*, 1–24. (d) Andrieux, C. P.; Hapiot, P.; Savéant, J.-M. *J. Phys. Chem.* **1988**, *92*, 5992–5995. (e) Parker, V. D. *Acta Chem. Scan. B* **1983**, *37*, 871–877.

(22) Olmstead, M. L.; Nicholson, R. S. *Anal. Chem.* **1969**, *41*, 851–852.

These K[Ru(OEP)(*Im)(H)] data are much more consistent with a second-order process than a first-order process but do not unequivocally prove a dimerization mechanism.

DPSCA of the K[Ru(TMP)(THF)(H)] yielded data with significantly more scatter than seen for the OEP complexes. However, the second-order rate constants extracted from these experiments were much lower (25 M^{-1} s^{-1}) than that for either of the OEP complexes.

To determine the experimental lower limit of rate constants that could be measured with our system, DPSCA was performed on K[Ru(OEP)(Me)], a structural analogue of the hydrides but known to be stable in both the II and III oxidation states. DPSCA experiments with this system should yield a second-order rate constant of zero. Any non-zero value will be due to non-idealities in our experiment. Values obtained from these experiments yielded a "second-order rate constant" of 7 M^{-1} s^{-1}. This non-zero rate is probably due to vibrations in the inert atmosphere box, uncompensated resistances, and problems with cell geometry. All of our second-order rate constants were significantly above this measured rate and thus can be used as good approximations of the reaction rates.

Discussion

General Synthesis of the Hydrides. Synthesis of the metalloporphyrin hydrides of ruthenium and osmium has been found to be quite general for any of the porphyrins that can withstand reducing conditions: OEP, TTP, and TMP. The metalloporphyrin dianions, $M(Por)^{2-}$, have a much greater basicity than their corresponding hydrides, $M(Por)(H)^-$. Consequently, acids which protonate $M(Por)^{2-}$ to the hydride but do not protonate $M(Por)(H)^-$ are readily available. Water is a convenient acid because in low relative concentrations, i.e., 10 equiv (≈30 mM), the dianion is immediately protonated to the hydride, but no dihydrogen is liberated within the span of hours. However, at relative concentrations of 1000 equiv, complete liberation of hydrogen is noted within hours. This allows easy access to the hydride without having to carefully control the stoichiometry.

Attempts to synthesize the hydride with benzoic acid failed. Benzoic acid showed little discrimination in attacking the dianion or the resulting hydride and produced a mixture of products. An especially convenient protonation reagent is *tert*-butyl chloride because its weak acidity will only allow protonation to the hydride. Additionally, upon elimination of the proton from *tert*-butyl chloride, isobutylene is formed and can easily be removed from the solution. Thus, no alkaline products, such as those formed from standard Brönsted acids, are produced. This is important because we have not been able to chromatograph or recrystallize the highly reactive hydrides.

The hydrides formed with THF at the axial coordination site, K[M(Por)(THF)(H)], are not soluble in aromatic or hydrocarbon solvents. The axial THF could not be detected in the ^1H NMR spectrum because of rapid exchange with the solvent but could easily be replaced with stronger axial ligands. This methodology was first used for rhodium porphyrin hydrides by Wayland,[23] and we have found that it provides a general route to a variety of axially ligated metalloporphyrin hydrides. Additionally, the presence of axial pyridine, imidazole, or triphenylphosphine ligands makes the metal hydrides soluble in toluene and benzene. All of the metalloporphyrin hydrides are extremely air-sensitive and readily decompose in the presence of chlorinated solvents.

Protonation of the Anionic Hydrides. To determine whether there was any bimolecular component to the protonation route of dihydrogen elimination, protonation of K[Ru(OEP)(L)(H)] with L = THF and pyridine was carried out with excess D_2O. In both cases, no H_2 was formed. Because D_2 was formed in approximately half the yield of HD (upon protonation of K[Ru(OEP)(THF)(H)]), we conclude that exchange between the D_2O and the hydride is occurring but that this process takes place more slowly than hydrogen elimination. Because hydrogen elimination is faster than H–D exchange, the absence of H_2 clearly rules out the bimolecular pathway as the predominant route for dihydrogen elimination in this system.

Dihydrogen formation through prior protonation of the site trans to the hydride would necessarily require a bimolecular step and would be expected to produce detectable amounts of H_2. Consequently, our results suggest that the dihydrogen elimination reaction is proceeding through protonation of the metal–hydride bond to form a dihydrogen complex intermediate that rapidly decomposes. The putative η^2-dihydrogen complex intermediate has been isolated at low temperature.[3] Such protonation of the metal hydride is expected to be kinetically favored over protonation at the metal, because hydride protonation requires neither a change of formal oxidation state nor a change in coordination number.[2]

Bimolecular elimination of hydrogen is also precluded following the protonation of K[Ru(OEP)(py)(H)] with D_2O because only HD was formed. Unlike the protonation of K[Ru(OEP)(THF)(H)], however, no exchange was observed between the D_2O and K[Ru(OEP)(py)(H)]. We have two explanations for this observation: (1) excahnge occurs via a *trans*-dihydride intermediate formed by opposite face protonation and the more tenaciously bound pyridine shuts off the opposite face to protonation, or (2) exchange occurs via a dihydrogen complex intermediate through protonation of the metal hydride bond, but because pyridine accelerates the hydrogen elimination reaction, the exchange reaction may not be competitive. Given our evidence, we cannot distinguish between these mechanisms.

Heterolytic Activation of H_2. The microscopic reverse of metal–hydride protonation resulting in dihydrogen elimination is the activation of H_2 in the presence of a metal to yield a metal hydride and a proton. We have effected this transformation by treating $Ru(OEP)(THF)_2$ with KOH and H_2 to form K[Ru(OEP)(THF)(H)]. This hydride is a good reducing agent both by hydride transfer (to the nicotinamide) and by 1 e^- transfer (−1.15 V vs. $FeCp_2^{+/0}$). Heterolytic H_2 activation has been reported for several transition metal complexes,[1] but this is the first proven example of such a hydride reducing an NAD^+ analogue.[24] This activity is important for the design of synthetic hydrogenases.

The hydride transfer from K[Ru(OEP)(THF)(H)] to the nicotinamide occurs specifically to form the 1,6-dihydropyridine, which is the expected thermodynamic product, rather than 1,4-dihydropyridine, which is the product resulting from the reduction of NAD^+ catalyzed by hydrogenase enzymes. We considered the possibility that the 1,6-dihydropyridine could have been formed by an initial 1,4-hydride transfer followed by a rapid [1,3]-sigmatropic H shift. The fact that $Ru(OEP)(THF)_2$ does not isomerize the 1,4-dihydropyridine to the thermodynamically more stable 1,6-dihydropyridine strongly suggests that initial hydride transfer occurs 1,6. This hypothesis is supported by the observation that deuterium was incorporated specifically at the 6 position of the ring when K[Ru(OEP)(THF)(D)] was used as the reducing reagent.

Even though the hydride transfer from K[Ru(OEP)(THF)(H)] yielded a different isomer of the dihydropyridine than the corresponding reduction with hydrogenase enzymes, it is interesting to note that dihydrogen can be heterolytically activated by a transition metal and reduce an NAD^+ analogue. This sequential heterolytic hydrogen activation and hydride transfer can be summarized as follows:

$$Ru(OEP)(THF)_2 + H_2\ KOH \rightarrow K[Ru(OEP)(THF)(H)] + H_2O$$

$$K[Ru(OEP)(THF)(H)] + NAD^+ \rightarrow 1,6\text{-NADH} + Ru(OEP)(THF)_2$$

$$H_2 + KOH + NAD^+ \rightarrow 1,6\text{-NADH} + H_2O \quad (8)$$

We believe that this type of mechanism for nicotinamide reduction

(23) Wayland, B. B.; Balkus, K. J.; Farnos, M. D. *Organometallics* **1989**, *8*, 950–955.

(24) Metal hydrides have been suggested in catalytic NAD^+ and NAD^+ model compound reductions. (a) Ruppert, R.; Herrmann, S.; Steckhan, E. *J. Chem. Soc., Chem. Commun.* **1988**, 1150–1151. (b) Aoyama, Y.; Midorikawa, K.; Toi, H.; Ogoshi, H. *Chem. Lett.* **1987**, 1651.

may play an important role in the catalyzed reduction of cofactors by hydrogen using hydrogenase enzymes. This idea was first proposed in 1954 by Krasna and Rittenberg,[4] but had not been previously demonstrated in the literature.[24,25]

The role that pyridine plays in the stoichiometric reduction of the pyridinium by the ruthenium(II) hydride is unclear. It is likely that the addition of the stronger axial ligand increases the hydride donor character of the metal hydride complex. This is consistent with the observation that changing the axial ligand of the anionic ruthenium(II) hydride from THF to pyridine also accelerated the rate of hydrogen evolution upon protonation. We have not attempted to determine the mechanism of the transfer of the hydride to the pyridinium salt but note that hydride transfers from anionic metal hydrides are common and have been mechanistically scrutinized.[26] The two mechanistic possibilities are direct hydride transfer or electron transfer followed by H atom transfer. In this specific system, the reduction potentials of the hydride (−0.6 V vs NHE) and the nicotinamide (reductions of nicotinamides occur ca. −0.75 V vs. NHE)[27] suggest that prior electron transfer is unlikely because of the unfavorable net potential. This suggests that the mechanism is direct hydride transfer. However, electron transfer followed by H atom transfer cannot be ruled out because the −0.15 V potential for the prior electron transfer results in a small equilibrium concentration of the one-electron reduced NAD^+. Subsequent, rapid H atom transfer could drive the unfavorable electron transfer equilibrium. This behavior has been detected for hydride abstraction from rhenium alkyls.[28]

Electrochemical Studies of Bimolecular H_2 Elimination. The cyclic voltammetry and DPSCA data demonstrate that upon oxidation of K[Ru(OEP)(THF)(H)] the rate of Ru(OEP)(THF)(H) decomposition is consistent with second-order kinetics. Some scatter is evident in the data, but the data are clearly inconsistent with a first-order decay. The data for K[Ru(OEP)(*Im)(H)] are also strongly suggestive of a bimolecular mechanism. The second-order rate constants for the chemical decomposition following the oxidation of these hydrides are (mean $\pm 2\sigma$) 88 ± 14 and 290 ± 110 M^{-1} s^{-1}, respectively. Considerably more scatter exists for K[Ru(OEP)(*Im)(H)], but the data clearly indicate that the imidazole ligand, with its stronger trans effect[29] than THF, accelerates the decomposition. The additional scatter is likely due to the *Im ligand exchanging with THF solvent (evident from its broad lines in the ^1H NMR spectrum in THF-d_8 solution). We will limit our discussion of the mechanism to the K[Ru(OEP)(THF)(H)], for which the data show less scatter.

The second-order kinetics has two possible origins: either (1) following oxidation, two ruthenium(III) hydrides approach each other and reductively eliminate dihydrogen (eq 9), or (2) following

$$2K[Ru(OEP)(THF)(H)] - 2e^- \rightarrow 2Ru(OEP)(THF)(H) \rightarrow H_2 + 2Ru(OEP)(THF)_2 \quad (9)$$

oxidation, the resulting ruthenium(III) hydride is deprotonated by a remaining ruthenium(II) hydride in a bimolecular fashion and the resulting H-free ruthenium(I) porphyrin formed in this step is subsequently oxidized (eq 10).[30] We have distinguished between these two mechanisms by utilizing an idea published by Hanafey.[31]

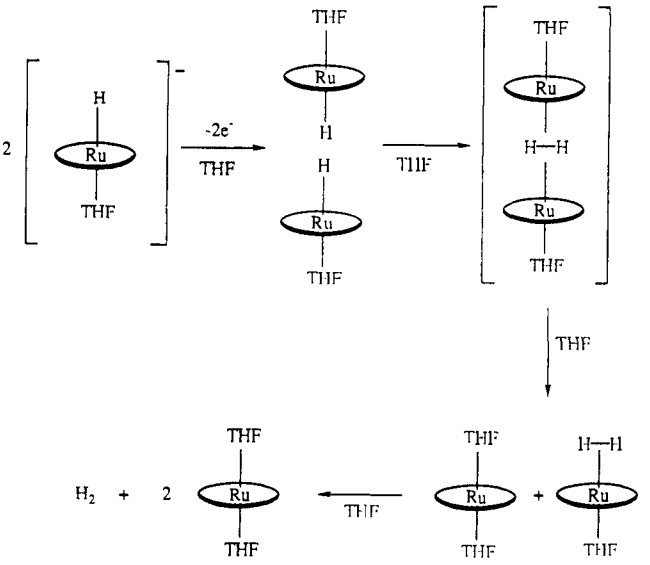

Figure 4. Proposed mechanism for bimolecular dihydrogen elimination from ruthenium porphyrin hydrides.

$$2K[Ru(OEP)(THF)(H)] - 1e^- \rightarrow K[Ru(OEP)(THF)(H)] + Ru(OEP)(THF)(H)$$

$$K[Ru(OEP)(THF)(H)] + Ru(OEP)(THF)(H) \rightarrow H_2 + K[Ru(OEP)] + Ru(OEP)(THF)_2$$

$$K[Ru(OEP)] - 1e^- \rightarrow Ru(OEP)(THF)_2 \quad (10)$$

Hanafey has pointed out that two different mechanisms may often display similar DPSCA behavior in a single region of the kinetic parameter (Figure 3), but generally these different mechanisms can be distinguished by evaluation of the data in several regions of the kinetic parameter. With our system, data can be obtained in different regions of the kinetic parameter by performing experiments for several values of the switching time, τ. If eq 10 were the operative mechanism, then the rate of decomposition should be dependent on the quantity of K[Ru(OEP)(THF)(H)] remaining in the diffusion layer. Performing the potential step experiment for a series of different stepping times, τ, has the effect of changing the relative concentration of the anionic hydride in the diffusion layer and should therefore allow us to differentiate between the processes shown in eqs 9 and 10.

We saw no systematic variation of second-order rate constants (for the chemical step following the oxidation of K[Ru(OEP)(THF)(H)] for different stepping times (Table II). This suggests that the mechanism in eq 9 is more likely.[32] Additional data favoring this mechanism have been obtained from the ^1H NMR investigation of the reactivity of K[Ru(OEP)(THF)(H)] following its low-temperature oxidation and subsequent warming in the NMR probe. After oxidation, none of the anionic hydride remained, yet the putative ruthenium(III) hydride decomposed to yield the η^2-dihydrogen complex.

The mechanism we suggest for the formation of dihydrogen is depicted in Figure 4. This approach of two ruthenium(III) hydrides to form dihydrogen sandwiched between two porphyrins, as an intermediate or transition state, would involve a complex that is analogous to the previously reported cofacial metallodiporphyrin bridging dihydrogen complex $Ru_2(DBP)(*Im)_2(H_2)$.[8b] This analogy lends further support to this mechanism.

(25) Dihydrogen complexes have been shown to act in the hydrogenation of acetone and olefins. (a) Harman, W. D.; Taube, H. *J. Am. Chem. Soc.* **1990**, *112*, 2261–2263. (b) Bianchini, C.; Mealli, C.; Meli, A.; Peruzzini, M.; Zanobini, F. *J. Am. Chem. Soc.* **1988**, *110*, 8725–8726. (c) Marinelli, G.; Rachidi, I.; Streib, W. E.; Eisenstein, O.; Caulton, K. *J. Am. Chem. Soc.* **1989**, *111*, 2346–2347. (d) Jackson, S. A.; Hodges, M.; Poliakoff, M.; Turner, J. J.; Grevels, F. W. *J. Am. Chem. Soc.* **1990**, *112*, 1221–1233.

(26) An excellent review of hydride transfers from transition metal hydrides has recently appeared. Bullock, R. M. *Comments Inorg. Chem.* **1991**, *12*, 1–33.

(27) Underwood, L.; Burnett, R. W. In *Electroanalytical Chemistry*; Bard, A. J., Ed.; Marcel Dekker: New York, 1973; Vol. 6, pp 1–86.

(28) Bodner, G. S.; Gladysz, J. A.; Nielsen, M. F.; Parker, V. D. *J. Am. Chem. Soc.* **1987**, *109*, 1757–1764.

(29) Collman, J. P.; Hegedus, L. S.; Norton, J. R.; Finke, R. G. *Principles and Applications of Organotransition Metal Chemistry*, 2nd ed.; University Science Books: Mill Valley, CA, 1987; pp 241–244.

(30) This behavior has been noted for formation of a dihydrogen complex upon oxidation of $(\eta^5\text{-}C_5H_5)Ru(CO)(PPh_3)H$. Ryan, O. B.; Tilset, M.; Parker, V. D. *Organometallics* **1991**, *10*, 298–304.

(31) Hanafey, M. K.; Scott, R. L.; Ridgway, T. H.; Reilley, C. N. *Anal. Chem.* **1978**, *50*, 116–137.

(32) The microscopic reverse of this reaction has been studied for Rh(TMP), i.e., $2(TMP)Rh^{\bullet} + H_2 \rightleftharpoons 2(TMP)Rh\text{-}H$. The rate law for this reaction is the following: rate = $k_1[(TMP)Rh^{\bullet}]^2[H_2]$. Wayland, B. B.; Ba, S.; Sherry, A. E. *Inorg. Chem.* **1992**, *31*, 148–150.

This mechanism, oxidatively induced bimolecular reductive elimination, is also supported by the result that the *Im ligand trans to the hydride accelerates the observed rate, as would be expected from its greater trans effect. Additionally, though the product stoichiometry from the oxidation of K[Ru(TMP)(THF)(H)] was not quantitative for dihydrogen formation, the fact that this decomposition is retarded, relative to the analogous decomposition of the less bulky OEP complex, is consistent with the bimolecular mechanism. Because the oxidation potentials for both the TMP metal hydride and the OEP metal hydride are nearly identical (Table I), the most likely explanation for the slower rate of dihydrogen elimination for the TMP complex relative to the OEP complex is their relative bulk. Because the steric repulsion encountered during coupling of two TMP metal hydrides likely increases the lifetime of the reactive metal hydride, hydride elimination from Ru(TMP)(THF)(H) may occur through different mechanisms than the one shown in Figure 4. These slow kinetics might also allow competing, non-hydrogen-forming, decomposition reactions to predominate. This may explain the poor product stoichiometries in the TMP reaction. Such a dependence of the rate of dihydrogen elimination, from two metal hydride centers, on the ability of the metals to obtain the correct transition state geometry has previously been seen for ferrocene derivatives.[33]

Factors Controlling Dihydrogen Elimination from Metal Hydrides. Several factors were found to affect the rate and mechanism of hydrogen evolution from metalloporphyrin hydrides. (1) *Oxidation state*: Though the ruthenium(III) hydrides readily eliminate dihydrogen, the anionic ruthenium(II) hydride, K[Ru(OEP)(THF)(H)], was found to be very resistant to reductive elimination. In fact, the reverse reaction is facile, i.e., $K_2[Ru(OEP)]_2$ homolytically cleaves dihydrogen to yield two molecules of ruthenium(II) hydride. Thus, bimolecular hydrogen evolution from ruthenium porphyrins likely only occurs through the ruthenium(III) hydrides. This curious change in reactivity upon oxidation likely reflects a dependence of the metal–hydride bond strength on the oxidation state of the metal. (2) *Axial ligation*: The addition of ligands, trans to the hydrides, with increasing trans effects leads to enhanced rates both for bimolecular hydrogen elimination from the ruthenium(III) hydrides and for unimolecular hydrogen elimination through protonation of the ruthenium(II) hydrides. (3) *Central metal*: Bimolecular elimination of dihydrogen from the osmium(III) hydride is approximately 100 times slower than bimolecular elimination from the corresponding ruthenium(III) hydride. Room temperature protonation of an osmium(II) hydride yields a dihydrogen complex[3] which slowly liberates dihydrogen, whereas protonation of the corresponding ruthenium(II) hydride results in immediate dihydrogen formation. Comparison of the isoelectronic hydrides K[Ru(OEP)(THF)(H)] and Rh(OEP)(H) reveals that only Rh(OEP)(H) will reductively eliminate dihydrogen.[23] This may be due to the lack of Coulombic repulsion experienced in the bimolecular rhodium–hydride transition state relative to the anionic ruthenium–hydride transition state. (4) *Steric bulk of the porphyrin*: Elimination of dihydrogen from ruthenium(III) porphyrins was slowed by addition of steric bulk (mesityl substituents of TMP) to the porphyrin ligand which is consistent with the proposed bimolecular mechanism.

The control of the rate of dihydrogen elimination will be important for the development of proton reduction catalysts. Slow rates of hydrogen elimination will allow decomposition reactions to compete with the hydrogen-evolving reaction. This is amply displayed by the reaction stoichiometries that have been analyzed in this work. Our poorest product yields were obtained for the slowest reactions, i.e., the hydrogen evolution from Os(OEP)(H) and Ru(TMP)(H). We suspect that H atom transfer reactions compete with slow bimolecular reductive eliminations. For catalytic processes, side reactions, especially those which cause catalyst degradation, are especially undesirable. Clearly, rapid hydrogen-evolving reactions, which do not allow competing reactions to occur, will be required of any catalyst.

(33) Hillman, M.; Michaile, S.; Feldberg, S. W.; Eisch, J. J. *Organometallics* **1985**, *4*, 1258–1263.

Two cobalt macrocycles reported to catalyze the reduction of protons in aqueous solution act partly through bimolecular reductive elimination of dihydrogen.[6,7] Enhancement of this rate of hydrogen elimination will be desired to prevent catalyst degradation reactions. We have shown that steric bulk of the porphyrin slows the rates of bimolecular dihydrogen elimination. If the porphyrins can be held in a proximal and suitable geometry, perhaps this rate can be greatly enhanced. Face-to-face porphyrins may be candidates to hold two metals in the proper geometry to enhance hydrogen formation and to retard such side reactions. Our group is currently investigating several biphenylene bridged cofacial metallodiporphyrins, M_2(DPB), to investigate the effect of catalyst geometry on hydrogen-elimination reactions.

Conclusions

A series of metalloporphyrin hydrides which shows strong reducing capabilities has been synthesized. One of these hydrides, K[Ru(OEP)(THF)(H)] (which is formed by heterolytic activation of hydrogen), reduces an NAD^+ analogue and thus serves as a good reactivity mimic of hydrogenase enzymes. These hydrides have also been induced to eliminate dihydrogen by either protonation of the metal hydride or oxidatively induced bimolecular reductive elimination. Analyses of the rates and stoichiometries of the bimolecular dihydrogen eliminations suggest that in order to inhibit side reactions, the rate of hydrogen elimination should be accelerated. Herein, we have suggested several methods for controlling these rates, i.e., modification of axial ligation, modifying the d-electron count and nature of the central metal, and controlling the steric bulk and proximity of the metal centers. Designing proton-reduction catalysts will necessarily require maximizing the effects of all of these modifications.

Experimental Section

General Considerations. Commercially available solvents and reagents were purchased and used as received unless otherwise noted. Solvents and reagents for use in the inert atmosphere box were further purified before use. Toluene, benzene, and THF were distilled under argon from sodium benzophenone ketyl. After introduction into the inert atmosphere box, these solvents were purged for 15 min with the box atmosphere to remove any residual oxygen. Tetrahydrofuran intended for routine use was monthly repurified in small amounts by vacuum transfer from its sodium benzophenone ketyl solution. THF for electrochemical experiments was vacuum transferred within days of performing the experiments. All other liquid reagents were degassed in Schlenk-ware by 3 freeze–pump–thaw cycles before introduction into the box. Aldrich *tert*-butyl chloride was passed through a plug of alumina (neutral activity) before degassing. Deuterated solvents were scrupulously dried prior to use in the inert atmosphere box. Benzene-d_6, toluene-d_8, and tetrahydrofuran-d_8 were purified by forming the Na/K benzophenone ketyl in a Schlenk flask and vacuum transferring to another Schlenk flask for storage. THF-d_8 was redried every 2 weeks. Tetrabutylammonium hexafluorophosphate was twice recrystallized from ethanol, dried in a vacuum oven (10^{-2} Torr, 100 °C), and stored in the inert atmosphere drybox. Ferrocene was purified by sublimation before use and $[FeCp_2]PF_6$ was synthesized according to literature procedures.[34]

All manipulations of the metalloporphyrin hydrides were performed in a Vacuum/Atmospheres Co. inert atmosphere drybox equipped with an HE493 Dri-Train and operated under an argon atmosphere. Oxygen levels (≤5 ppm) were monitored by a Vacuum/Atmospheres Co. AO316-C trace oxygen analyzer. Solvent manipulations and degassing of air-sensitive samples were performed on a bench top vacuum line in Schlenk flasks and NMR tubes fitted with J-Young Teflon valves and O-ring vacuum adapter fittings. ^1H NMR data were recorded on Varian XL-400 and GEM-200 instruments. All electrochemical experiments were carried out in the inert atmosphere box using a Princeton Applied Research 175 wave generator and the 173 Potentiostat/Galvanostat. The working electrode (platinum disk, $r \approx 0.5$ mm) was circumscribed by the platinum wire loop auxiliary electrode in a 2-mL compartment that was separated from the reference electrode by a Luggin capillary. The reference electrode was typically a Ag wire and was referenced to ferrocene at the conclusion of the experiment. The value of ferrocene vs. NHE was calculated with use of published data.[35] Unless otherwise noted, all

(34) Yang, E. S.; Chan, M.-S.; Wahl, A. C. *J. Phys. Chem.* **1975**, *79*, 2049–2052.

(35) Bard, A. J.; Faulkner, L. R. In *Electrochemical Methods: Fundamentals and Applications*; John Wiley and Sons, Inc.: New York, 1980; pp 699–702.

electrochemical experiments were carried out in THF with 0.2 M TBA-PF_6 as the backing electrolyte. The metalloporphyrins were present in mM concentrations. CV and DPSCA data were plotted in real time on an HP X-Y recorder.

Quantification of Hydrogen Isotopes. Separation of H_2, HD, and D_2 was achieved utilizing an HP 5890 gas chromatograph with a thermal conductivity detector (TCD). The column used was prepared by a modification of the literature procedures.[36] Activated alumina (30–60 mesh) was impregnated with 10% by weight $MnCl_2$ by dissolving the $MnCl_2$ in ethanol, adding the alumina, and rocking the slurry in a shallow pan with a stream of warm air passing over it until the ethanol evaporated. The paramagnetic $MnCl_2$ serves to equilibrate ortho and para hydrogen. After air drying, the alumina was packed into a 7 ft piece of $^1/_8$ in. o.d. Cu tubing which had been rinsed inside with methylene chloride. The column was coiled to a 2 in. diameter. A stainless steel tube ($7 \times {}^1/_8$ in. o.d.) was packed with 40–60 mesh CuO (ground from Aldrich reagent CuO wire and sized using meshing screens) and mated with Swagelok fittings to the alumina column. The purpose of the CuO column is to convert the hydrogen isotopes to their oxides so that they are more readily detected by the TCD. The column was mounted in the GC with the alumina end connected to the injector port and the CuO end connected to the TCD. The column was activated with flowing He (30 mL/min, 100 °C, 24 h). For use, the alumina column was submerged in liquid N_2, and the CuO catalyst column was heated to 350 °C using heating tape. Using a flow rate of 30 mL/min He, the retention times for H_2, HD, and D_2 were 7.5, 9, and 12 min, respectively, with baseline separation. When 1:1 mixtures of H_2:D_2 in Ar were injected onto the column, their responses were identical (±1%), suggesting that no correction factor need be applied for differences in thermal conductivity of H_2O, HDO, and D_2O. Several injections of the same sample also gave a high degree of precision (±0.5%) with respect to the ratios of the three isotopes.

Typical DPSCA Analysis. One milliliter of a 2 mM solution of K[Ru(OEP)(THF)(H)] in 0.2 M $TBAPF_6$/THF was admitted into the working electrode compartment of the electrochemical cell. A cyclic voltammogram was performed on the solution to determine that the system was performing well and to determine the oxidizing and reducing potentials for the DPS experiments. The stepping potentials were chosen as ca. 400 mV positive and negative of E_{pa} and E_{pc}, respectively ($E_{pa} - E_{pc} \approx 80$ mV). DPSCA experiments were then recorded for forward stepping times, τ, ranging from 2 to 20 s. The vertical scale was chosen to maximize the signal on the X-Y recorder for each step. The cell was then emptied and refilled with an identical solution and the experiments repeated. To obtain the background currents, the cell was emptied, rinsed, and refilled with only the electrolyte solution and the experiments repeated. Current ratios, $i_r(t+\tau)/i_f(t)$, for t/τ values of 0.3 were obtained by measuring the currents and subtracting out the corresponding background currents. For example, if τ is 10 s, the current from the background trace at 3 s into the forward step was subtracted from the current at 3 s into the forward step of the hydride. The same was done for 3 s into the reverse potential step. Finally, the reverse current was divided by the forward current. Current ratios from each of the two identical runs were averaged, and kinetic parameters were obtained from the theoretical working curves. Rate constants were derived from these first- and second-order kinetic parameters.

In Situ Preparation of the Anionic Hydrides. K[Ru(OEP)(THF)(H)], K[Os(OEP)(THF)(H)], and K[Ru(TMP)(THF)(H)] were prepared according to the literature methods[10,11] via protonation of K_2[M(Por)]. Excess (3–10 equiv) H_2O or *tert*-butyl chloride was added to millimolar solutions of K_2[M(Por)] in THF. Typically, 5 μmol of the hydride was formed in 1 mL THF solution. The solutions were filtered to remove residual KOH and KCl formed in the protonation reaction, and the solvent was removed by reduced pressure evaporation. ^{1}H NMR data matched the previously reported data and showed porphyrinic impurities ≤5%. The hydrides were used immediately, and all subsequent stoichiometries and kinetics were based on the assumption that the hydride was obtained quantitatively.

K[Ru(OEP)(THF)(D)]. K_2[Ru(OEP)] was produced from 3.0 mg (2.4 μmol) of [Ru(OEP)]$_2$ by the literature method[10] and was then protonated in situ with 1 μL of D_2O (56 μmol, 12 equiv/Ru). The solution was filtered and the solvent removed by reduced pressure evaporation. ^{1}H NMR (THF-d_8) showed no visible protium in the hydride position.

K[Ru(OEP)(*Im)(H)]. A 1-mL THF solution containing K[Ru(OEP)(THF)(H)] (4.8 μmol) was treated, while being stirred, with 1-*tert*-butyl-5-phenylimidazole (*Im; 4.8 μmol, 1 equiv) from a stock solution (44 mM). The solvent was removed and the resulting residue was soluble in toluene and benzene. ^{1}H NMR (tol-d_8, ppm): porphyrinic resonances, H_{meso} 8.02 (s, 4 H), CH_2 3.33 (q, 16 H), CH_3 1.54 (t, 24 H); imidazole resonances, *p*-phenyl 6.41 (t, 1 H), *m*-phenyl 6.24 (t, 2 H), *o*-phenyl 5.46 (d, 2 H), $H_{imidazole}$ (obscured), *tert*-butyl −0.23 (br, 9 H); Ru-H −47.5 (br, 1 H).

K[Ru(OEP)(py)(H)]. K[Ru(OEP)(THF)(H)] was dissolved in pyridine, which was found to immediately displace the THF. The solvent was removed by reduced pressure evaporation. ^{1}H NMR (THF-d_8, ppm): porphyrinic resonances, H_{meso} 8.22 (s, 4 H), CH_2 3.47 (m, 16 H), CH_3 1.66 (t, 24 H); pyridine resonances, H_p 5.76 (t, 1 H), H_m 4.81 (t, 2 H), H_o (not seen); Ru-H −49.3 (v br).

K[Ru(OEP)(py)(D)]. The deuteride with a trans pyridine was prepared analogously to the hydride.

K[Ru(OEP)(PPh$_3$)(H)]. A stirred 1-mL THF solution containing K[Ru(OEP)(THF)(H)] (4.8 μmol) was treated with PPh_3 (4.8 μmol, 1 equiv) from a stock solution. The solvent was removed by reduced pressure and the resulting residue was soluble in toluene and benzene. ^{1}H NMR (C_6D_6, ppm): porphyrinic resonances H_{meso} 7.97 (s, 4 H), CH_2 3.26 (m, 16 H), CH_3 1.46 (t, 24 H); triphenylphosphine resonances, H_p 6.43 (br, 3 H), H_m 6.23 (br, 6 H), H_o 4.43 (br, 6 H); Ru-H −37.8 (d, J_{PH} = 176 Hz); ^{31}P NMR (C_6H_6) −1.51 ppm vs. H_3PO_4 (d, J_{PH} = 176 Hz).

Treatment of [Ru(OEP)]$_2^{2-}$ with H_2. [Ru(OEP)]$_2$ was partially reduced in THF-d_8 with a small bead of potassium. ^{1}H NMR showed a species which matched the known spectrum of K_2[Ru(OEP)]$_2$.[10] The solution was also contaminated with K_2[Ru(OEP)]. The solution in the NMR tube was saturated with dihydrogen using a syringe needle. The NMR tube was capped under 1 atm of H_2 and sonicated in a cleaning bath (Bransonic Cleaning Equipment Co. Model No. B-2200R-1) for 30 min. A subsequent ^{1}H NMR spectrum showed the formation of K[Ru(OEP)(THF)(H)] and the disappearance of K_2[Ru(OEP)]$_2$.

Ru(OEP)(THF)$_2$ was prepared according to the literature procedure.[10] Under Ar, [Ru(OEP)]$_2$ was dissolved in freshly purified THF (1–2 mg/mL) and placed into a 1 × 10 cm quartz glass Schlenk tube fitted with a J. Young valve and an O-ring joint. A small magnetic stir bar was also added. The solution was degassed and photolyzed (Conrad-Hanovia 450 W medium pressure Hg vapor UV lamp housed in a water cooled quartz glass jacket) while being stirred and cooled with a stream of air for 20 min. ^{1}H NMR (THF-d_8, ppm) H_{meso} 9.29 (s, 4 H); CH_2 3.88 (q, 16 H); CH_3 1.83 (t, 24 H); THF ligands not observable.

Ru(OEP)(*Im)(THF). [Ru(OEP)]$_2$ (2.4 μmol) was dissolved in 1 mL of THF and stirred vigorously while 4.8 μmol (1 equiv/Ru) of *Im from a stock solution (44 mM in toluene) was added slowly with a syringe. The THF was removed to yield a residue of Ru(OEP)(*Im)(THF) that was contaminated with small amounts of Ru(OEP)(*Im)$_2$ and Ru(OEP)(THF)$_2$. ^{1}H NMR (THF-d_8, ppm): porphyrinic resonances, H_{meso} 9.07 (s, 4 H), CH_2 3.78 (m, 16 H), CH_3 1.76 (t, 24 H); imidazole resonances, *p*-phenyl 6.91 (t, 1 H), *m*-phenyl 6.74 (t, 2 H), *o*-phenyl 5.91 (d, 2 H), $H_{imidazole}$ 1.52 (s, 1 H), $H_{imidazole}$ 1.05 (s, 1 H), *tert*-butyl 0.11 (s, 9 H).

Ru(OEP)(PPh$_3$)(THF). Ru(OEP)(PPh_3) was prepared by the literature method[10] of adding 2 equiv of triphenylphosphine to [Ru(OEP)]$_2$ in benzene. The monotriphenylphosphine complex was then dissolved in THF. ^{1}H NMR (THF-d_8, ppm): porphyrinic resonances, H_{meso} 9.23 (s, 4 H), CH_2 3.81 (m, 8 H), CH_2 3.73 (m, 8 H), CH_3 1.80 (t, 24 H); triphenylphosphine resonances, H_p 6.65 (t, 3 H), H_m 6.34 (t, 6 H), H_o 4.04 (t, 6 H).

1-Benzyl-*N*,*N*-diethylnicotinamide, Hexafluorophosphate Salt. The chloride salt of 1-benzyl-*N*,*N*-diethylnicotinamide was prepared by a modification of the procedure for preparation of 1-benzyl-nicotinamide chloride.[37] Five milliliters of *N*,*N*-diethylnicotinamide was refluxed for 3 h in 50 mL of neat benzyl chloride. Cooling afforded white crystals of the chloride salt which were washed with acetone. Anion exchange was achieved by dissolving 0.5 g of the chloride salt in 3 mL of H_2O and adding a saturated solution containing 2 g of KPF_6. A tan oil formed and was extracted with CH_2Cl_2 and dried over $MgSO_4$. The solvent was removed and the oil was crystallized from methanol/H_2O. The white crystals were washed with H_2O and dried. ^{1}H NMR (THF-d_8, ppm): phenyl resonances, 7.4–7.6 (m, 5 H); ethyl resonances, CH_2 3.52 (q, 2 H), 3.31 (q, 2 H), CH_3 1.21 (t, 3 H), 1.11 (t, 3 H); pyridinium resonances, H2 9.06 (s, 1 H), H4 8.52 (d, 1 H), H5 8.12 (t, 1 H), H6 8.96 (d, 1 H); benzylic proton, CH_2 5.87 (s, 2 H).

1-Benzyl-*N*,*N*-diethyl-1,6-dihydronicotinamide. The 1,6-dihydronicotinamide was prepared from [1-benzyl-*N*,*N*-diethylnicotinamide]Cl according to the literature method.[38] ^{1}H NMR (THF-d_8, ppm): phenyl resonances, 7.1–7.4 (m, 5 H); ethyl resonances, CH_2 3.32 (q, 4 H), CH_3

(36) (a) Walters, A. B. Ph.D. Dissertation, Stanford University, 1970. (b) Paonessa, R. S.; Prignano, A. L.; Trogler, W. C. *Organometallics* **1985**, *4*, 647–657.

(37) Büchi, G.; Coffen, D. L.; Kocsis, K.; Sonnet, P. E.; Ziegler, F. E. *J. Am. Chem. Soc.* **1966**, *88*, 3099–3109.

1.08 (t, 6 H); dihydropyridine resonances, H1 7.00 (s, 1 H), H4 6.04 (d, 1 H), H5 4.88 (td, 1 H), H6 3.87 (d, 2 H); benzylic protons, CH_2 4.21 (s, 2 H).

1-Benzyl-*N*,*N*-diethyl-1,4-dihydronicotinamide. The 1,4-dihydronicotinamide was prepared as an impure mixture with the 1,6-dihydronicotinamide from the [1-benzyl-*N*,*N*-diethylnicotinamide]Cl according to the literature method for 1-methyl-*N*,*N*-diethyl-1,4-dihydronicotinamide.[38] ^{1}H NMR (THF-d_8): phenyl resonances, 7.2–7.4 (m, 5 H); ethyl resonances, CH_2 3.29 (q, 4 H), CH_3 1.02 (t, 6 H); dihydropyridine resonances, H1 6.16 (s, 1 H), H6 5.84 (d, 1 H), H5 4.50 (td, 1 H), H4 3.05 (d, 2 H); benzylic protons, CH_2 4.24 (s, 2 H).

Hydride Transfer to NAD$^+$ Analogue. K[Ru(OEP)(THF)(H)] (ca. 5 μmol) was treated with 1 mL of a THF-d_8 solution containing [1-benzyl-*N*,*N*-diethylnicotinamide]PF_6 (1.2 mg, 2.9 μmol, <1 equiv). The ^{1}H NMR showed that in addition to the unreacted K[Ru(OEP)(THF)(H)], a species with broad ^{1}H NMR signals was present. A drop of pyridine-d_5 added to the solution produced the known Ru(OEP)$(py)_2$ and the dihydronicotinamide. The spectrum of the latter matched the ^{1}H NMR spectrum given above for 1-benzyl-*N*,*N*-diethyl-1,6-dihydronicotinamide.

Deuteride Transfer to NAD$^+$ Analogue. K[Ru(OEP)(THF)(D)] (7.4 μmol) was dissolved in THF and treated with 3.1 mg of [1-benzyl-*N*,*N*-diethylnicotinamide]PF_6 (7.5 μmol, 1 equiv). Two drops of pyridine were added and the solvent was then removed under reduced pressure. The residue was dissolved in THF-d_8 and the ^{1}H NMR showed Ru(OEP)$(py)_2$ and signals consistent with deuterium substituted in the 6 position of the 1-benzyl-*N*,*N*-diethyl-1,6-dihydronicotinamide. In particular, the 5 H proton at 4.88 ppm, which appears as a triplet of doublets in the full protio species, appeared as a doublet of doublets with a very small (<2 Hz) triplet coupling imposed on the peaks.

Determination of the Products Resulting from K[M(Por)(L)(H)] Oxidation. K[M(Por)(L)(H)] (4.8 μmol) was dissolved in 500 μL of THF-d_8. $Me_3SiSiMe_3$ (1 μL) was added as an internal NMR standard. The ^{1}H NMR spectrum was recorded and the porphyrin signals were integrated relative to the internal standard. In the inert atmosphere box, a 1-dram vial fitted with a mini-inert syringe valve was charged with a stir bar and the solid oxidant. When $[FeCp_2]PF_6$ was used as the oxidant, 1.6 mg (1 equiv) was used. If VBr_3 was used as the oxidant, 2–3 mg (1–2 equiv) was used. The NMR sample was syringed into the vial and stirring was initiated. After 30 min a 0.2-mL sample of the headspace was removed and analyzed for H_2 by GC. The NMR sample was then filtered to remove excess oxidant and any solid decomposition products, and a ^{1}H NMR spectrum was then recorded and integrated. The porphyrin signals were matched to known porphyrins, and their yield was calculated on the basis of relative integration, versus the standard, before and after the oxidation.

Low-Temperature Oxidation and NMR of K[Ru(OEP)(THF)(H)]. A 21-μL concentrated solution of $[FeCp_2]PF_6$ (0.21 M) in CH_3CN was carefully loaded into the top of a horizontally held NMR sample tube fitted with a rotationally balanced J-Young valve (there is an indentation just below the point where the Teflon valve seals which serves as a good reservoir for small solvent volumes). The solvent was removed under reduced pressure, leaving a residue of $[FeCp_2]PF_6$ (4.4 μmol) around the top of the tube. A 600-μL solution of K[Ru(OEP)(THF)(H)] (4.4 μmol) was carefully added to the bottom of the NMR tube with a long pipet. The NMR tube was sealed with the valve, brought out of the drybox, and cooled in a dry ice/acetone bath. The XL-400 NMR probe was cooled to −60 °C while shimming on a standard THF-d_8 sample. The NMR tube containing the reagents was then shaken to allow complete mixing and immediately plunged into the probe. The probe was then slowly warmed to room temperature, recording a spectrum every 15 °C. The predominant initial species had a temperature-dependent paramagnetic spectrum. ^{1}H NMR (THF-d_8): (−60 °C) δ 9.76 (br, 8 H, CH_2), 9.26 (br, 8 H, CH_2), −3.62 (br, 24 H, CH_3), −9.45 (br, 4 H, meso-H); (−15 °C) δ 9.84 (br, 16 H, CH_2), −2.30 (br, 24 H, CH_3), −3.96 (br, 4 H, meso-H); the paramagnetic species had entirely decomposed by the time the probe had warmed to room temperature.

(38) Schmidt, R. R.; Berger, G. *Chem. Ber.* **1976**, *109*, 2936–2947.

Appendix

Olmstead and Nicholson[22] have published a table in which a potential step current function, $\phi(y)$, is tabulated versus the kinetic parameter $y_s = k_2C_0^*\tau$, for a series of $y/y_s = t/\tau$, where k_2 is the second-order rate constant, C_0^* is the initial concentration of the electroactive species, τ is the duration of the first potential step, and t is the time into the second potential step (measured from $t = 0$ at the beginning of the first potential step) for which $\phi(y)$ is being measured. The kinetic parameter, y_s, is in the proper form for our x-axis. However, we desire the y-axis to simply contain the current ratio, i_r/i_f. In the above paper, $\phi(y)$ is related to the current in the return step by the following relationship:

$$i_r = nFA(k_2C_0^*D_0)^{1/2}C_0^*\phi(y)$$

We know the current at t_f into the forward step as the Cottrell current:

$$i_f = nFAD_0^{1/2}C_0^*/(\pi t_f)^{1/2}$$

The current ratio i_r/i_f is then:

$$i_r/i_f = \phi(y)[\pi k_2C_0^*t_f]^{1/2}$$

Substitution of

$$k_2C_0^* = y_s/\tau$$

gives

$$i_r/i_f = \phi(y)[\pi y_s t_f/\tau]^{1/2}$$

Finally, if $t_f = t_r - \tau$, that is if we analyze the currents in each pulse at the same time into their respective pulse, then $t_f/\tau = y/y_s - 1$. Substitution gives:

$$i_r/i_f = \phi(y)[\pi y_s(y/y_s - 1)]^{1/2}$$

Plotting i_r/i_f vs y_s for a series of y/y_s values gives a series of curves similar to those in Figure 3 and analogous to the first-order plots given by Schwarz and Shain.[20]

Acknowledgment. We acknowledge Professor Robert Hembre for first suggesting that we analyze these compounds for hydrogenase enzyme reactivity. We thank Professor Royce Murray, Professor Jack Norton, and Jim Hutchison for helpful suggestions. Dr. Scott Bohle and Cindy Kellen are thanked for their help in the preparation of this paper. We thank the National Science Foundation, the National Institutes of Health, and the Gas Research Institute for financial support. This is contribution No. 8520 from the Division of Chemistry and Chemical Engineering, California Institute of Technology.